Nanoscale Advances

ROYAL SOCIETY OF CHEMISTRY

PAPER

View Article Online
View Journal | View Issue

Cite this: *Nanoscale Adv.*, 2021, **3**, 725

Dendronized vesicles: formation, self-organization of dendron-grafted amphiphiles and stability†

Akash Banerjee, Acacia Tam ‡ and Meenakshi Dutt *

Fundamental bacterial functions like quorum sensing can be targeted to replace conventional antibiotic therapies. Nanoparticles or vesicles that bind interfacially to charged biomolecules could be used to block quorum sensing pathways in bacteria. Towards this goal, dendronized vesicles (DVs) encompassing polyamidoamine dendron-grafted amphiphiles (PDAs) and dipalmitoyl-*sn*-*glycero*-3-phosphocholine lipids are investigated using the molecular dynamics simulation technique in conjunction with an explicit solvent coarse-grained force field. The key physical factors determining the stability of DVs as a function of the dendron generation and relative concentration are identified. The threshold concentration of each dendron generation that yields stable DVs is determined. Dendrons with lower generations rupture the DVs at high relative concentrations due to the electrostatic repulsions between the terminally protonated amines. Whereas, dendrons with intermediate generations demonstrate a mushroom-to-brush transition. Conformational changes in the dendrons expand the outer DV surface, resulting in instability in the DV bilayer. DVs encompassing dendrons with higher generations incur stresses on the bilayer due to their high charge density and spontaneous curvature. The self-organization of PDAs on the DV surface are examined to understand how the asymmetric stresses are minimized across the bilayer. A set of conditions are determined to be conducive for the formation of a single cluster of PDAs that decorates the DV surface like a mesh. Results from this study can potentially guide the design and synthesis of nanoparticles which target quorum sensing pathways in bacteria towards the prevention and treatment of bacterial infections. Furthermore, these nanoparticles can be used in diverse applications in biomedicine, energy or electronics that require synthetic dendronized cells or the adsorption and transport of charged species.

Received 15th September 2020
Accepted 19th December 2020

DOI: 10.1039/d0na00773k

rsc.li/nanoscale-advances

Introduction

Multi-drug resistance towards conventional antibiotic therapies has led to the innovation of alternate strategies to treat bacterial infections.[1,2] These strategies include approaches that are predicated on the interception of fundamental bacterial functions such as quorum sensing.[3,4] Quorum sensing is the ability to discern and respond to variations in cell population density through the regulation of genes. Quorum sensing is typically facilitated by the production of autoinducer (AI) molecules. When these AIs reach a critical threshold, they interact with suitable receptors. This process alters the gene expression in the participating bacteria, enabling the production of biofilms[5] or toxic metabolites. The toxic metabolites are produced by communication between cells which is dependent upon the cell density. The suppression of quorum sensing can occur *via* the disruption of the synthesis of the AIs through interference with synthase enzymes; destruction of the AIs and hindering their buildup, and blocking the receptors.[2]

Nanoparticles play an instrumental role in disrupting quorum sensing[6,7] by ceasing the communication between the bacteria without any toxic side effects to the biological cells in the host.[8] The design of the nanoparticles along with their drug loading abilities prescribes the precise mechanism for the inhibition of quorum sensing. Hyperbranched polyelectrolyte-based nanoparticles (*e.g.*, dendrimers) have been shown to attenuate the signaling molecules enabling quorum sensing.[8] Earlier studies have shown dendrimer-like complexes loaded with anti-quorum sensing agents to block the receptor protein which regulates the gene expression[9] enabling biofilm production. Furthermore, these polyelectrolyte-based dendrons can interfere with the activity of the enzymes to suppress the synthesis of the AIs. Dendrimer-like complexes disrupt the extracellular polymeric substances (EPSs) that constitute majority of organic matter in biofilms.[10] Dendrimers associate

Chemical and Biochemical Engineering, Rutgers, The State University of New Jersey, Piscataway, NJ 08854, USA. E-mail: meenakshi.dutt@rutgers.edu

† Electronic supplementary information (ESI) available: Equilibrated bilayer, bilayer-to-bicelle transition, migration of dendrons towards bicelle edge, asymmetric distribution of dendrons in the DV bilayer, scaling exponents for qualitative comparison against polymer theory, packing factor calculations. See DOI: 10.1039/d0na00773k

‡ Present addresses: Meinig School of Biomedical Engineering, Cornell University, Ithaca, NY 14853.

with the EPSs and cause membrane disruption.[10] In addition, the positively charged moieties at the periphery of cationic dendrons disrupt bacterial cell membranes *via* favorable electrostatic interactions.[11] Therefore, nanoparticles decorated with polyamidoamine (PAMAM) dendrons have the potential to be highly effective in intercepting quorum sensing pathways. In addition, these characteristics of the dendrons could make them potentially useful for anti-fouling applications. Also, these dendrons are administered with antibiotics[8] to increase the efficacy of the latter. In the future, nanoparticles encompassing suitably functionalized polyelectrolyte-based dendrons which disrupt quorum sensing and are toxic to bacteria may replace antibiotics to treat bacterial infections. Such an approach would address the growing resistance to antibiotics. This study focuses on designing nanoparticles, or vesicles, which can disrupt quorum sensing with the ultimate goal of stemming bacterial infection.

Experimental studies demonstrate the formation of stable vesicles constituted of generation 1 PAMAM dendrons grafted to two alkyl tails.[12] The addition of the alkyl tails in dendron-grafted amphiphiles is motivated by their ability to enhance fusion with the plasma membrane and self-assemble into nanostructures.[13] The former increases the potency of anti-virulence mechanisms that are predicated upon intake into the cytoplasm. The favorable interactions between nucleic acids[13] and hyperbranched polyelectrolytes extends the functionality of these nanostructures to a broad range of applications. These vesicles are susceptible to structural modifications in acidic or basic environments due to the PAMAM dendrons.[11,12] The sharp increase in the charge density of the dendrons with higher generations significantly changes the physical properties of the hyperbranched polyelectrolytes.[14] Dendrons with higher generations are highly effective in transfecting cells.[15] However, amphiphiles encompassing dendrons with higher generations have yet to be investigated for their ability to form stable, self-assembled nanostructures.[12,13,16,17]

Computational studies demonstrate the impact of pH on the conformation of PAMAM dendrimers.[18] The effect of pH is incorporated into the model for the PAMAM dendrimer by varying the protonated states of the constituent primary, tertiary amines and amide groups. The radius of gyration of the PAMAM dendrimers is found to increase in acidic environments.[11,19] Other studies use free energy calculations to measure the favorable interactions between PAMAM dendrimers and phospholipid bilayers.[20]

In this study, the stability of vesicles encompassing PAMAM dendron-grafted amphiphiles (PDAs) and dipalmitoyl-*sn*-glycero-3-phosphocholine (DPPC) phospholipids is examined. The molecular species are selected due to the ability of hyperbranched polyelectrolytes to disrupt quorum sensing and the alkyl tails to enhance fusion of the vesicles with the plasma membrane. Vesicles encompassing phospholipids and PDAs ranging from generations one through six are created through the membrane closing process. The self-organization of the dendron-grafted amphiphiles in the vesicle bilayer during the process is observed to impact the stability of the vesicles. The threshold concentration of the PDAs for each dendron generation at which stable vesicles are formed is identified. In addition, the factors disrupting the stability of the vesicles at higher relative concentrations and generations of the PDAs are determined. A set of conditions inducing the formation of a single cluster of PDAs that decorates the DV surface like a mesh is reported. The predicted designs from this study can be used to inspire and guide the synthesis of nanoparticles which could potentially intercept the quorum sensing pathway in multiple ways, thereby catalyzing innovative anti-virulence strategies that bypass drug resistance. The results from this study can motivate diverse applications in biomedicine, energy and electronics which require synthetic dendronized cells, or the adsorption and transport of charged species.

Methods

Vesicles encompassing mixtures of DPPC phospholipids and PDA are examined. DPPC was selected due to its biocompatibility as it is lung surfactant.[21] DPPC has been extensively used in many computational[22–24] and experimental studies[25–28] and hence, its physico-chemical properties are well characterized. In addition, a DPPC membrane is in the gel state at physiological temperatures which makes it suitable for forming stable vesicles which encompass amphiphiles with bulky water soluble head groups.[25–30] The characteristics of the vesicles encompassing molecular species with different relative concentrations and generations of the dendrons (namely, generation 1 (G1) through generation 6 (G6)) are studied. The dynamics of the system is resolved over extensive spatiotemporal scales *via* the molecular dynamics (MD) simulation technique used in conjunction with the explicit solvent coarse-grained (CG) Martini force field.[31] The non-bonded interactions are defined by the Lennard-Jones and coulombic electrostatic potentials. The cut-off distance for both potentials is set at 1.2 nm. Large periodic simulation boxes ($50 \times 50 \times 50$ nm^3) are generated to host vesicles that have dimensions (diameter: 22.1 nm) comparable to experimental observations.[32,33] Since these systems consist of approximately a million particles, long range electrostatics has not been incorporated. The simulation time increases by a factor of 6 with particle mesh Ewald summation (PME)[34,35] for long range electrostatics (using an optimal Fourier spacing). This would significantly slow down the investigation (from the perspective of computational cost) of a large phase diagram encompassing several dendron generations and relative concentrations. Also, Fig. S1† compares the effect of long range electrostatics on one of the measurements reported in this paper. This comparison shows that there is minimal impact on the measured values when long range electrostatics is incorporated in the model. Details of this comparison will be discussed at the end of the Results and discussion section.

The GROMACS MD package[36,37] (version 2016.4) is used to generate particle trajectories for characterization of the system. To ensure reproducibility of the results, each observable is averaged using four independent particle trajectories.

The CG representation of DPPC is derived using a phospholipid database.[38] The PDAs encompass alkyl tails which are

identical to those of the DPPC phospholipids. Each alkyl chain for the DPPC and PDA consists of four C1 type beads. The hydrophobic tails will promote the assembly of DPPC and PDA molecules. The two alkyl tails in the PDAs are connected to the innermost tertiary amine of the dendrons. The bonded interaction parameters for the PAMAM dendrons is based upon an earlier study on dendrimers.[15] In comparison to lipid bond and angle parameters, a higher force constant is used for the dendrons. This allows the dendron branch to maintain its rigid structure and excluded volume, independent of the PDA relative concentrations.

The CG representation for the PAMAM dendrons (see Fig. 1B–G) is based upon earlier studies.[15,39] The dendrons encompass primary, tertiary amines and amide groups. The primary amines are the terminal end groups of the dendron branch. The pH determines the protonated state of each of these chemical moieties. Under neutral pH conditions the terminal end groups are protonated.[12] The repulsions between the positively charged terminal end groups are expected to induce swelling of the branches. Hence, the terminal groups are represented by a Qd bead type, which represents a hydrogen bond donor moiety with a unit positive charge. The amide groups represent the amide linkage between the branching points (tertiary amines) and terminal groups (primary amines). The amide group has mild polarity and is represented by a P3 bead type.[19,40] The inner most layer of the dendrons consists of tertiary amines. The tertiary amines are nonpolar and are represented by a N0 bead type. The charge neutrality of the system is maintained through chloride counterions. The Qa bead type (namely, unit negative charge with hydrogen bond accepting capability) is used to model the chloride ions.

To validate the PAMAM dendron model, the measurements of the radius of gyration (R_g) for a G5 dendrimer[15,41] are compared with corresponding measurements from experimental[42,43] and other computational studies.[15] The radius of gyration is evaluated using the following equation

$$R_g^2 = \frac{\sum_{i=1}^{N} M_i r_i^2}{\sum_{i=1}^{N} M_i}$$

where N is the number of dendrimer beads, r_i is the distance of the i^{th} bead from the center of mass of the dendrimer and M_i is the mass of the i^{th} bead.

The model for the G5 dendrimer is based upon prior studies.[15,39,40] Additional solvation in the interior section of the dendrimer is included by assigning mild polarity to the amide groups[19,40] to induce moderate inner swelling of the branches. This feature allows the radius of gyration to increase and thereby, agree with previously reported experimental data. As an aside, an all atom computational study on dendrimers and phospholipid membranes reports lower exterior surface hydration of the branches,[41] resulting in the adsorption of the dendrimers onto the phospholipid membrane surface. As discussed later, the interfacial adsorption of small dendrons onto the phospholipid bilayer is observed extensively throughout this study.

A preassembled bilayer encompassing 3040 DPPC lipids in a simulation box with dimensions $30 \times 30 \times 4$ nm^3 is generated. The height of the simulation box is expanded from 4 nm to 10 nm to accommodate the water beads. The bilayer remains stable as its hydrophobic region is not exposed to the solvent. Particle overlaps are removed *via* 5000 steps of energy minimization, using the steepest decent algorithm. The system is equilibrated in the canonical ensemble *via* a v-rescaling thermostat with a stochastic term[44] at temperature of 323 K. This

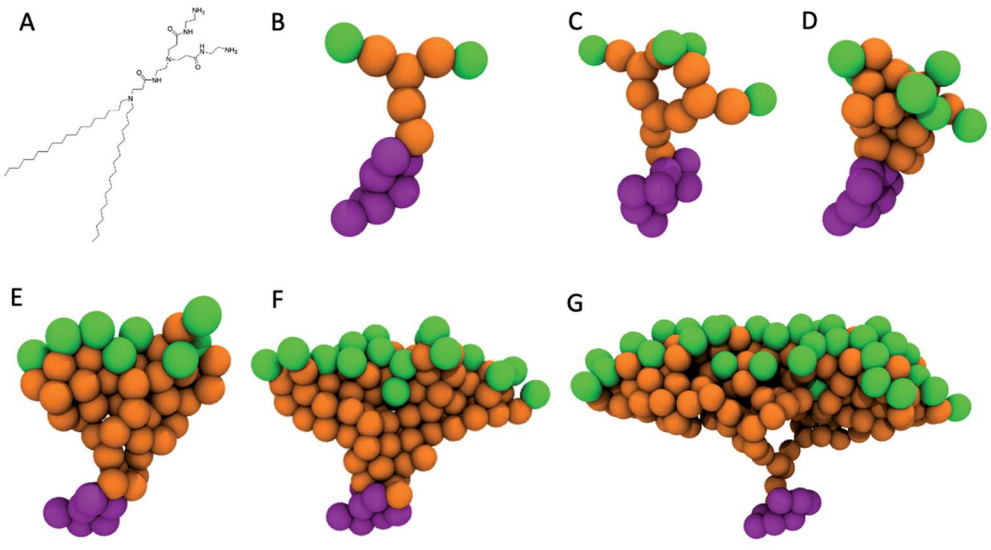

Fig. 1 The PAMAM dendron branch bearing 2 C_{18} alkyl chains is represented using the Martini coarse-graining scheme. (A) Chemical structure of G1 PAMAM dendron-grafted amphiphiles. (B–G) Coarse-grained models of generations 1 to 6 of PAMAM dendron-grafted amphiphiles. The orange beads represent the amide groups and tertiary amines of the dendron branches. The green beads represent positively charged terminal amines. The purple beads represent the lipid tails of the PAMAM dendron.

step is followed by further equilibrating the system in the NPT ensemble using Parrinello–Rahman barostat with semi-isotropic pressure coupling to maintain a pressure of 1 bar.

After the bilayer is equilibrated, a grid of a specific dimension is mapped onto the top and bottom surfaces of the bilayer. At each intersection of the grid lines, a lipid is selected as a grafting site. The head beads of the selected lipids are replaced by a PAMAM dendron. These grafted amphiphiles form the initial configuration of the PDAs. The system is equilibrated in the NPT ensemble for 400 ns to allow the dendrons to relax. The equilibrated bilayer with the PDAs (see Fig. S2†) is inserted into a larger simulation box such that the hydrophobic region of the bilayer edges is exposed to the solvent. This large box has dimensions of $50 \times 50 \times 50$ nm^3. Minimization of the interfacial energy initiates a process which yields either stable (Fig. 2A) or unstable dendronized vesicles (DVs) (Fig. 2B). Details of the process are discussed in the Results and discussion section. The system is equilibrated in the NPT ensemble for 400 ns using an isotropic pressure coupling barostat. Each system is simulated for 4 μs, followed by a 100 ns simulation to generate trajectories for analysis. A timestep of 20 femtoseconds is used for all production runs.

Results and discussion

The DVs are generated using the approach detailed in the Methods section. The role of dendron generation (*i.e.*, G1 through G6) and relative concentration on the characteristics of the DVs encompassing DPPC and PDAs is examined. For each generation, a corresponding relative concentration (*i.e.*, critical concentration limit) that yields stable DVs is identified. On increasing the relative concentration of PDAs beyond the critical concentration limit, mixed irregular assemblies with a ruptured membrane are observed. The structure and spatial organization of the dendrons, as a function of generation and relative concentration, provides insight into the key factors which induce membrane rupture. Lower generation dendrons (namely, G1 and G2) destabilize the DV bilayer by a significant increase in electrostatic repulsions. Intermediate generations (*i.e.*, G3 and G4) disrupt the bilayer *via* conformational changes in the dendron branches which impose local asymmetric stresses on the DV bilayer. Higher generations such as G5 and G6 rupture the bilayer *via* interplay between a significant increase in the dendron–lipid interactions and the spontaneous curvature of the dendrons. The former arises due to the high charge density of the dendrons.

Formation of dendronized vesicles

Using the process detailed in the Methods section, an equilibrated bilayer encompassing DPPC and PDAs (see ESI file Fig. S2†) with a specific dendron generation is created. The bilayer is placed at the center of a larger simulation box filled with water beads which exposes the hydrophobic section of the bilayer to the solvent. The exposure of the hydrophobic tails to water generates unfavorable interactions. These unfavorable interactions initiate two processes to minimize the interfacial energy: the amphiphilic molecules at the edges of the bilayer reorganize so as to shield the hydrophobic groups from the solvent, and the bilayer bends to fuse its edges. The former process transitions the bilayer into a bicelle.[45] The latter process transitions the bicelle into a vesicle.

The edge (see Fig. S3†) of the bicelle has a higher positive curvature[46] in comparison to its planar upper and lower surfaces, and hence provides excess surface area that is favorable for the excluded volume of the dendrons. However, the generation of the dendrons is observed to impact the diffusion of the PDAs across the bicelle. Fig. S4E† describes the average position of the dendrons on the bicelle. If the average position is farther from the center of the bicelle (radius = 0 nm), it would suggest that the dendrons may migrate towards the bicelle edge. In comparison to smaller dendrons (G2), the average position of intermediate dendrons (G3 and G4) is farther away

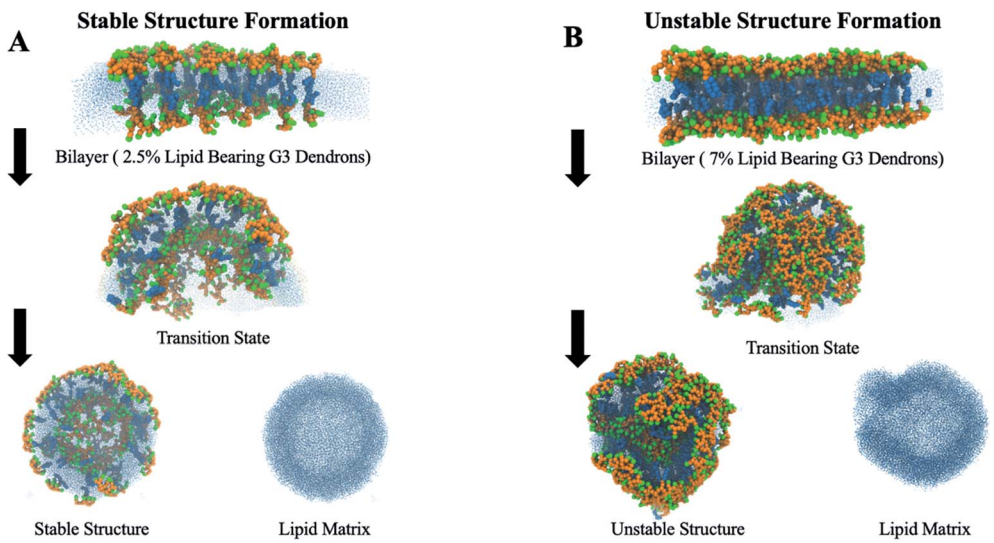

Fig. 2 The process of membrane closing from a stable bilayer to a (A) stable or (B) unstable vesicle.

from the center of the bicelle. It is difficult to resolve this trend with certainty given the statistical variability in the results. This type of grafted polymer chain displacement towards the outer edge of a bicelle has been reported in earlier computational[46] and experimental[47] studies. The PDAs with larger generations (*i.e.*, G5) do not migrate towards the edges of the bicelles (Fig. S4D†).

The bicelle is simulated in the NPT ensemble until the outer edge fuses to transition the bicelle into a DV (see Fig. 2). In some cases, as the dendrons are located at the edge of the bicelle, the PDAs are observed to be organized close to each other after the bicelle-to-vesicle transition. The displacement of the PDAs alters their local concentration. An increase in the concentration would result in conformational changes of the dendrons, and impose curvature on the DV surface. These changes will be discussed in subsequent sections.

Phase diagram of dendronized vesicles

Fig. 3 summarizes the morphologies of the stable DVs as a function of dendron generation and relative concentration. The critical concentration limit (see Table 1) for stable DVs is observed to reduce with the generation of the dendrons. The DVs encompassing PDAs with G2 and G3 dendrons have identical critical concentration limits. PDAs with G2 dendrons have a higher tendency to distribute themselves asymmetrically across the monolayers during the bicelle-to-vesicle transition process (see Table S1†). Prior to the commencement of the transition process, all the bilayers have the same number of PDAs on each monolayer. However, during the membrane closing process some PDAs may diffuse in the bicelle such that they locate themselves in the opposite monolayer after the formation of the DV. The outer monolayer can host higher relative concentrations of PDAs as the inner monolayer volumetrically constrains the dendrons. Hence, DVs will typically have a higher number of PDAs on the outer monolayer.

Characteristics of dendrons on dendronized vesicles

The molecular characteristics of the DVs are determined by an interplay of favorable and unfavorable electrostatic interactions. The favorable interactions arise between oppositely charged terminal protonated amines in the dendrons with the lipid polar groups.[15,20,41,48,49] These interactions induce the interfacial adsorption of a fraction of the terminal amines onto the lipid bilayer surface. The unfavorable interactions arise between the like-charged terminal protonated amines of neighboring dendrons,[50] and are predominantly responsible for their conformational changes at higher grafting densities. The contribution of each type of interaction on the characteristics of the DV is dependent on the generation and relative concentration of the PDAs.

For PDAs with lower generation dendrons (*i.e.*, G1 and G2), majority of the terminal protonated amines are interacting with the lipid polar groups on the surface of the DV. The impact of relative concentration of the PDAs on these interactions is negligible. Hence, the terminal groups of the dendrons are forced to interact laterally with corresponding groups from the neighboring dendrons. These observations are supported by comparisons of the favorable and unfavorable interaction counts (see Fig. 4A).

PDAs with intermediate dendron generations (*i.e.*, G3 and G4) demonstrate a reduction in the interactions between the terminal protonated amines and the lipid polar groups with increasing relative concentration, or local density (see Fig. 4A). The closer packing of the dendrons on the surface of the DVs would cause an overlap of their individual excluded volumes and induce unfavorable lateral interactions between the terminal protonated amines of the neighboring dendrons.[51] The terminal protonated amines extend away from the surface of the DV to reduce the overlap of their individual excluded volumes. These conformational changes reduce the interactions between the terminal protonated amines and the lipid polar groups.

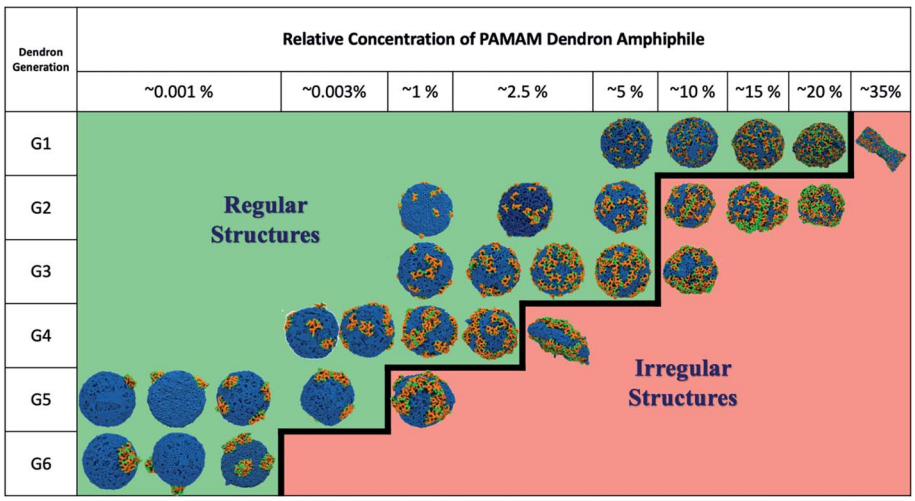

Fig. 3 Final assemblies of PDAs and DPPC lipids as a function of the generation and relative concentration of PDAs. The regular structures (stable vesicles) have been separated from the irregular structures by the black line. Color scheme: blue – DPPC lipids, orange – amide groups and tertiary amines in PAMAM dendrons and green – positively charged terminal amines.

Table 1 Key properties for different generations of PAMAM dendron-grafted amphiphiles at the critical concentration limit

Generation	Relative PDA concentration	Total number of terminal amines	Number of terminal amines in the outer monolayer
G1	20%	1296	760
G2	5%	648	380
G3	5%	1296	696
G4	2.5%	800	400
G5	0.005%	384	192
G6	0.0025%	512	256

However, the extended conformations at higher local densities of the dendrons also increases the interactions between the terminal protonated amines. The electrostatic interactions in higher generations of dendrons (namely, G5 and G6) are not sensitive to the relative concentration of PDAs (see Fig. 4A). This behavior arises due to the very low numbers of PDAs present in the DVs.

Earlier studies have suggested that higher grafting density of polymers would result in their conformation transitioning from a mushroom to a brush.[51–53] In this study, the dendrons are categorized to adopt mushroom-like conformations provided they occupy a volume equivalent to their excluded volume. The adoption of this conformation would be indicative of limited lateral interactions between neighboring dendrons. This conformation is typically observed at lower concentrations,[54] and can be assumed to occupy an effective hemispherical volume with a radius equivalent to the radius of gyration of an isolated, grafted dendron. When the relative concentration is increased beyond a threshold value, the PDAs would need to minimize the overlap of their excluded volume (and lateral

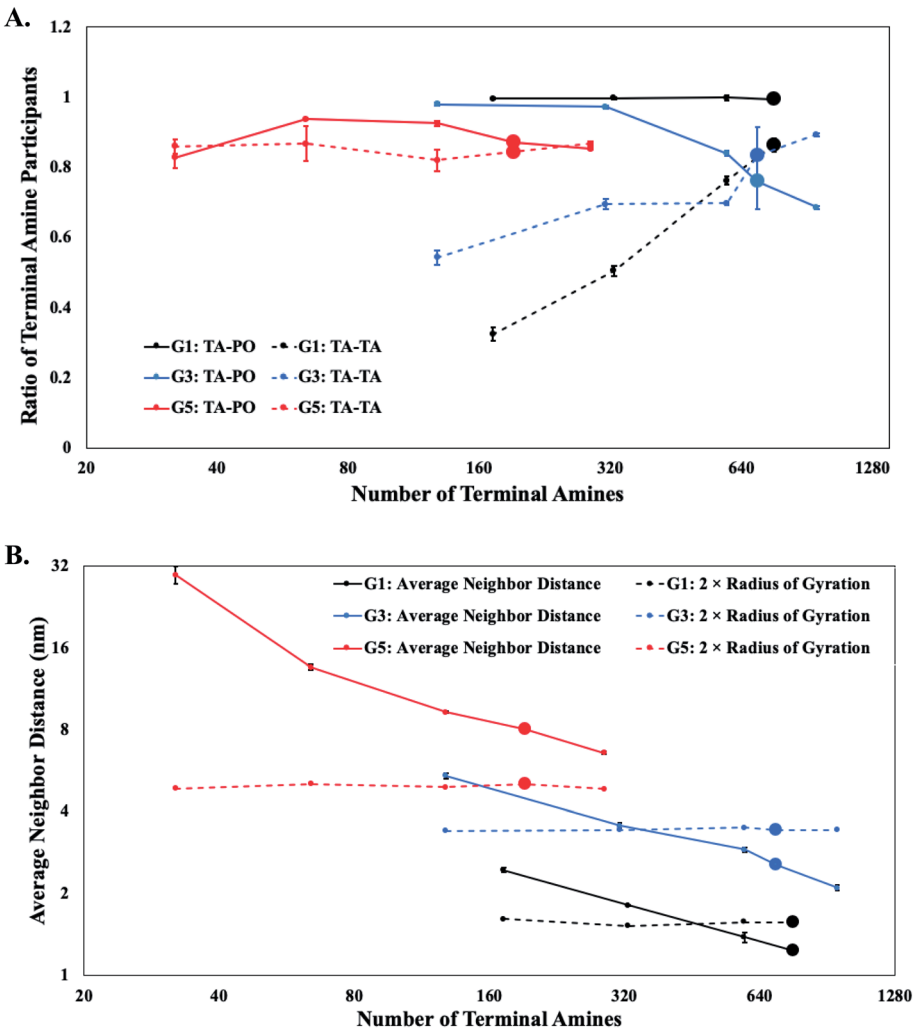

Fig. 4 (A) Interactions between the terminal amine beads of dendron branches and phosphate beads of DPPC lipids shown using solid lines (TA–PO). Interactions between the terminal amines shown using the dotted lines (TA–TA). The interactions are reported as a ratio of the number of terminal amines involved in the specific type of interaction to the total number of terminal amines in a PDA. The *x* axis is scaled using log of base 2 as most of the chosen relative concentrations are twice its previous value. (B) The average spacing between dendron grafting points as a function of the number of terminal amines shown using solid lines. An increase in terminal amines is equivalent to an increase in the relative concentration of the PDAs. The dotted lines denote twice the radius of gyration described by the terminal amines. Both axes are scaled using log of base 2. The enlarged data points represent the critical concentration limit corresponding to the dendron generation.

interactions) by diffusing to regions with a lower local density of dendrons, or by changing their conformations. Diffusion of a single PDA to a less densely populated region will be dependent upon the proximity and concentration of neighboring PDAs. If the PDA is unable to diffuse to a less populated region of the bilayer, the dendron branches will extend radially outwards (away from the DV bilayer) and adopt a brush-like conformation.[55] In addition, the repulsion between the terminal protonated amines of the dendrons will favor brush-like conformations. Majority of the dendrons are observed to adopt mushroom-like conformations for lower relative concentrations. However, at higher relative concentrations, only a fraction of the dendrons extend away from the bilayer to adopt brush-like conformations.

The conformation of the PDAs is categorized by determining the average distance of separation (D) between the dendron grafting points,[56] for different relative concentrations and generations. The value of D is evaluated for the PDAs on the outer monolayer, as dendrons emanating from the inner monolayer are volumetrically constrained. In addition, conformational changes in PDAs on the outer monolayer are predominately responsible for rupture of the DVs. The average distance of separation is compared to a characteristic length associated with the excluded volume of the dendrons adopting a mushroom conformation. The characteristic length is the radius of gyration (R_g) of isolated dendrons which is measured using the terminal amines. The lateral interactions and repulsions between the terminal protonated amines of neighboring dendrons are assumed to become significant when $D \leq 2R_g$ (where $2R_g$ is the diameter associated with the excluded volume of a dendron adopting a mushroom conformation). The average distance of separation becomes less than twice the radius of gyration for relative concentrations lower than the critical limit for lower (G1 and G2) and intermediate (G3 and G4) generations (see Fig. 4B). These observations indicate the conformation of the dendrons, for these generations and specific relative concentrations, to transition from a mushroom to a brush conformation. However, for larger generations (G5 and G6), the dendrons maintain mushroom conformations for all the relative concentrations (see Fig. 4B).

The changes in the structure of the dendrons are probed through the end to end distance. This calculation is noisy due to the favorable interactions between the terminal amines and lipid polar groups, and is supported by observations from other measurements. The end to end distance is given by the average Euclidean distance between every terminal amine and its corresponding grafting point, normalized by the ideal path length of the branch. The ideal path length is defined by the following relation: (number of beads between a terminal amine and the grafting point $-$ 1) $\times$ bond distance between two beads. The scaling exponent relating the end to end distance to the molecular weight indicates the degree of expansion or compression of the dendrons with increase in the relative concentration of the PDAs. The scaling exponent for lower generation (*i.e.*, G1 and G2) dendrons is approximately 0 (in Table S2†) which indicates minimal change in the extension of the dendron branches with relative concentration. This observation is supported by insignificant changes in the interactions between the terminal amine and lipid polar groups (see Fig. 4A). Both results indicate that the lower generation dendrons preferentially interact with the lipid polar head groups on the DV surface. This preferential interaction constrains the conformational flexibility of the dendrons resulting in a sharp increase in the interactions between the terminal amine groups of neighboring dendrons, for higher relative concentrations of PDAs. Increase in the concentration of PDAs results in the rupture of the DV bilayer. As per Table S2,† a positive scaling exponent for intermediate generations (*i.e.*, G3 and G4) indicates expansion of the dendritic arms and thereby, changes in their conformation. This observation is supported by the average neighbor distance measurements summarized in Fig. 4B.

Numerous experimental and theoretical studies on polymer-grafted surfaces utilize scaling relations between the height of the polymer brush (Z) and its molecular weight[50,52,54,55] to obtain insight into the interactions between and the relative conformation of the polymers as a function of their chain length. These studies focus on systems where the polymer does not interact with the surface. Due to the favorable interactions between the terminal amines and lipid polar groups, it is difficult to compare the scaling exponents for this system with corresponding measurements from prior studies.[50,52,54,55] However, the difference between the scaling exponents for polymers with and without interactions with the surface can be used to quantify the effect of the surface on the polymer conformation.

As majority of the dendrons have favorable interactions with the DV bilayer, the height is determined using the dendron branches that are extended away from the surface (see Fig. S6†). Earlier studies focusing on systems with no interactions between the polymer and the surface report the following relation: $Z \sim {M_w}^{0.5}$.[55] Scaling measurements for lower and intermediate dendron generations are determined to be respectively $Z \sim {M_w}^{0.28}$ and $Z \sim {M_w}^{0.02}$. The smaller scaling exponents indicate the reduced effect of the higher relative concentrations (or, higher molecular weights) on the conformations of the dendrons. The favorable interactions between the terminal amines and the lipid polar head groups restricts the conformational changes of the dendrons. In the absence of interactions between the dendrons and the surface, higher concentrations of dendrons resulted in an increase in the brush height to reduce lateral interactions between neighboring dendrons.[50] Similarly, the relation between the height of the dendron and the average spacing between two neighboring grafting points is given by $Z \sim D^{-0.623}$ and $Z \sim D^{-0.046}$ (Table S4†), respectively for lower and intermediate dendron generations. Comparison of these measurements with results ($Z \sim D^{-0.5}$) from a prior study[55] shows a higher relative concentration to result in lower average spacing. However, the favorable interactions between the terminal amines and the lipid polar groups significantly undermines the impact of higher concentrations.

A high density of dendrons at the bicelle edge during the formation of the DVs could potentially result in a single large

cluster of PDAs after the bicelle-to-vesicle transition. The interactions of the dendrons with each other and with the lipid polar groups could potentially induce localized asymmetric stresses in the DV bilayer, resulting in its rupture or in the formation of transient pores.[15] Hence, the projection area of the dendrons on the DV bilayer is characterized at higher concentrations towards understanding the impact of the PDA relative concentration on the stability of DVs.

The surface of a DPPC vesicle with the same number of molecules is used as a reference to determine the projection area of all the dendrons on the DV bilayer. This projection area includes the areas of overlap between the dendrons when $D < 2R_g$, and is called the true projected area. The true projected area is evaluated by counting the number of DPPC polar beads that are within interaction range from the dendron terminal beads. The product of the number of such interactions with the area of cross-section of each interaction provides the projected area of all the dendrons on the DV surface. This approach overestimates the true projected area as the projected area can vary between different dendrons due to their internal degrees of freedom. Therefore, a comparison of the true projected area with the theoretical projected area is required. The theoretical projected area is the projected area of the dendrons when $D > 2R_g$, independent of PDA concentration.

The true and theoretical area for different generations is provided in Fig. 5. The set of two lines intersect with each other only for intermediate dendron generations (*i.e.*, G3 and G4). This means that the true and theoretical projected areas are equal at a specific value of the relative concentration of the PDA. The true projected area becomes less than the theoretical projected area after the point of intersection, as neighboring dendron branches or their corresponding projected areas begin to overlap. The overlap of the dendron branches results in the formation of PDA clusters at higher values of the relative concentration of the dendrons. In most of the cases for the intermediate generations, majority of the dendrons aggregate into a single, large cluster (Fig. 6). This observation implies that the true projected area provides a good estimate of the surface area occupied by the single, large PDA cluster. This area can be assumed to be numerically representative of and therefore, proportional to the local asymmetric stress on the DV bilayer, induced by an aggregate of PDAs. Hence, as the true and theoretical projected areas are equivalent for intermediate dendron generations, majority of the dendron branches are assumed to be participating in a single, large cluster of PDAs (see Fig. 5, inset B). This large cluster will induce localized asymmetric stresses in the DV bilayer. In addition, if the true projected area becomes less than the theoretical projected area, the PDA cluster will become more compact (see Fig. 5, inset C) and induce larger localized asymmetric stresses in the DV bilayer. In contrast, dendron branches for the lower and higher generations have negligible overlap.

The true and theoretical projected areas of the dendrons increase with relative concentration of the PDAs. For intermediate dendron generations (*i.e.*, G3 and G4), the true projected area is observed to be equal to the theoretical projected area at a certain relative concentration (see Fig. 5). The dependence of the magnitude of the localized asymmetric stresses on the dendron generation can be obtained by comparing the critical relative concentrations for G3 and G4 dendrons. For G3 dendrons, the true projected area is observed to be lower than the theoretical projected area at the critical concentration limit. This implies that the G3 dendrons form a single large PDA cluster at a relative concentration smaller than the critical concentration limit (see Fig. 5, inset B). The PDA cluster becomes more compact at the critical concentration limit (see Fig. 5, inset C), generating larger local asymmetric stresses, and resulting in the rupture of the DV bilayer. Whereas, the G4 dendrons form a cluster that has a true projection area equivalent to the theoretical projection area at the critical concentration limit. At this relative concentration, the local asymmetric stresses generated are sufficiently large so as to rupture the DV bilayer. In this case, the cluster is not sufficiently compact. Hence, the comparison between G3 and G4 dendrons in the category of intermediate dendron generations identifies the dependence of the magnitude of the asymmetric stresses on the dendron generation. Therefore, dendrons with relatively lower generations aggregate into one single large cluster below the critical concentration limit. Due to the smaller branch sizes, the impact of the stress induced by the PDA cluster is not sufficient to spontaneously rupture the DV bilayer. However, for relatively larger dendrons, the DV bilayer experiences significantly higher asymmetric stresses when a single large PDA cluster is formed. This asymmetric stress instantaneously ruptures the vesicle.

For lower relative concentration of PDAs, the dendrons are dispersed on the DV bilayer. PDAs with higher dendron generation are not observed to form clusters, or have their excluded volumes intrude into the corresponding excluded volume of neighboring dendrons. Therefore, PDAs with higher generations are well dispersed across the DV bilayer. Yet, stable DVs are only able to accommodate low relative concentrations of PDAs with higher generations. This observation could be explained by the higher curvature induced by PDAs of higher generations. The curvature imposed by a single dendron is termed as spontaneous curvature.[57] Since the projected area measurement suggests that majority of the dendrons are dispersed across the DV bilayer, the spontaneous curvature induced by the dendrons with higher generations causes localized expansion of the bilayer[56,58] and therefore asymmetric stresses at multiple dispersed sites. The collective effect of the stresses at multiple sites could potentially result in the formation of transient pores and rupture of the DV bilayer. In addition, prior studies have suggested that the large charge density of dendrimers with higher generations plays an instrumental role in the formation of pores in bilayers.[59–61] This observation could be explained by a higher number of dendron–lipid interactions within a localized region of the DV bilayer. These interactions allow dendron branches to penetrate the bilayer and create pores.[15] Fig. 4A shows a constant number of dendron–lipid interactions for dendrons with higher generations. This observation implies that the dendrons branches consistently associate with the DV bilayer, independent of the relative concentration. At larger relative concentrations of dendrons

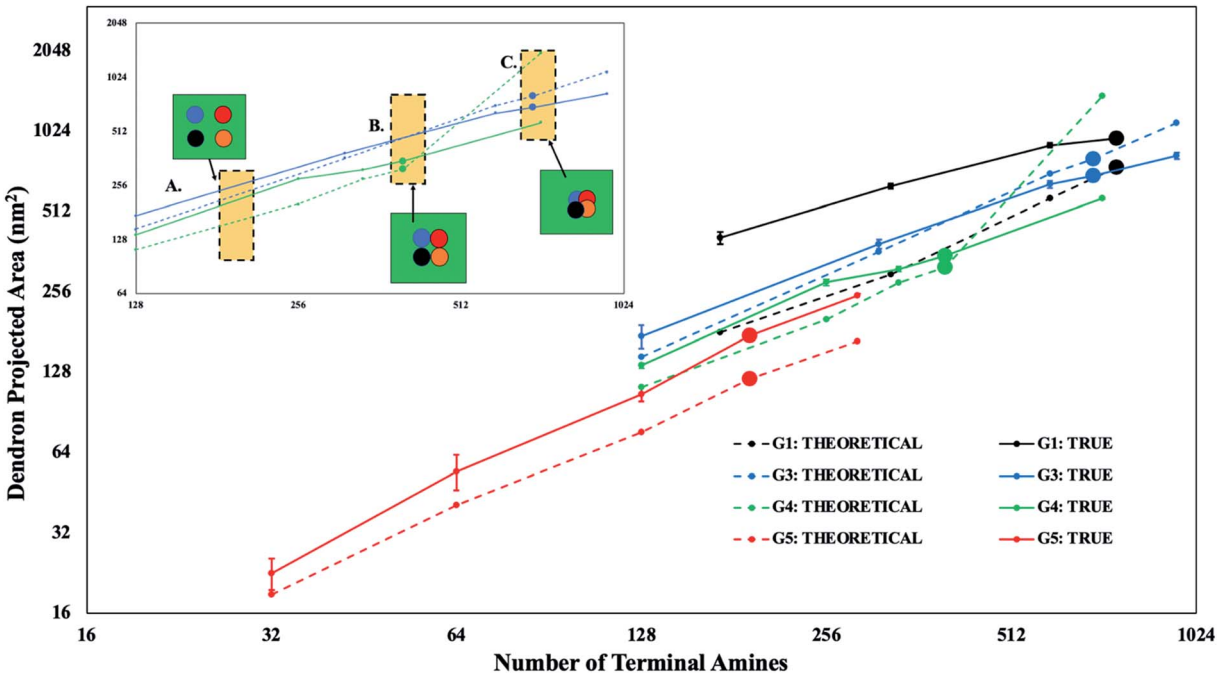

Fig. 5 The projected area of the dendron head beads on the DV surface as a function of the number of terminal amines. Solid lines represent the true surface area and dotted lines represent the theoretical surface area. The enlarged data points represent the critical concentration limit corresponding to the dendron generation. The *x* and *y* axes are scaled using log of base 2 as most of the chosen relative concentrations are twice their preceding value. Inset: a rectangular outer patch of the DV bilayer (in green color) consisting of four intermediate dendron branches has been depicted in A–C. Each dendron branch is denoted by a unique color (blue, black, red and orange). Inset A represents the initial state where every dendron has an excluded volume that is not overlapping with excluded volumes corresponding to neighboring dendrons. Inset B represents the scenario where the excluded volume of the dendrons begin to overlap and the dendrons begin to form a single cluster. Inset C shows the same cluster where the excluded volume of the constituent dendron branches is overlapping. The *x* and *y* axes of the inset are scaled to fit the values for intermediate dendrons.

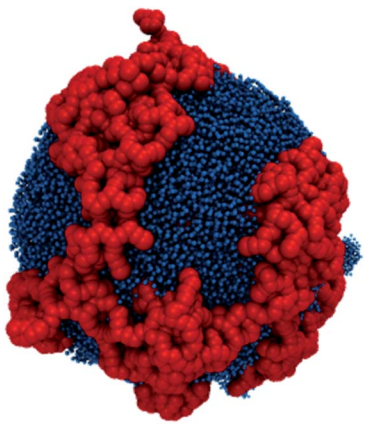

Fig. 6 A large cluster of G3 PAMAM dendrons on a DV (blue) has been shown in red color.

with higher generations, the dendron–lipid interactions could contribute to the disruption of the DV bilayer. Therefore, a larger density of dendron–lipid interactions coupled with spontaneous curvature effects could contribute to the rupture of DV bilayers encompassing dendrons with higher generations.

To understand the key factors which determine the distribution of PDAs in the DV bilayer as a function of generation and relative concentration, the average cluster size is measured. Fig. 4A suggests that electrostatic repulsions between terminal amines are limited for smaller relative concentrations of dendrons with lower and intermediate generations. Due to the lack of electrostatic repulsion between neighboring dendrons, it is surmised that the dendrons aggregate to localize the asymmetric stresses in the DV bilayer. However, the formation of a single, compact cluster encompassing all the PDAs in the system would generate significantly higher curvature which is localized in a specific region of the DV bilayer, resulting in its rupture. In Fig. 7, the size of dendron clusters is determined as a function of the interactions between the terminal protonated amines and lipid polar groups (*i.e.*, the dendron–lipid interactions). The *x*-axis has been normalized by the total number of interactions to permit comparisons across all dendron generations.

For dendrons with lower and intermediate generations (see Fig. 7), small clusters form when the dendron–lipid interactions are high. These favorable interactions are expected at low relative concentrations of the PDAs (see Fig. 4A). For lower number of dendron–lipid interactions, the clusters grow in size. This observation is attributed to the increasing relative concentration of PDAs. The negative correlation between dendron–lipid interactions and the cluster size could be explained by the decrease in dendron–lipid interactions which would decelerate

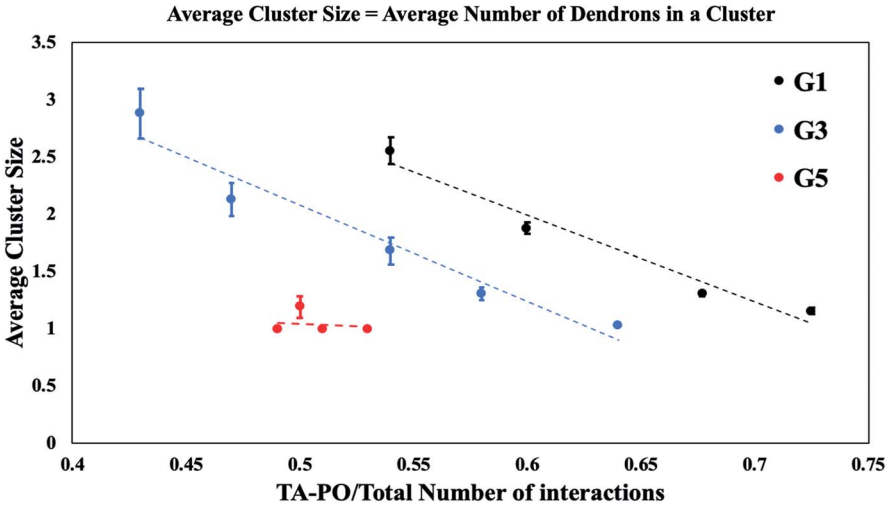

Fig. 7 The average cluster size of PDA aggregates as a function of the number of interactions between the terminal protonated amines and lipid polar groups (*i.e.*, dendron–lipid interactions). The value of the *x* axis has been normalized by the total number of interactions in each system. The unit for cluster size is dimensionless.

the process of pore formation, thereby stabilizing the vesicle. In addition, the decrease in the favorable dendron–lipid interactions is consistent with an increase in the repulsions between the terminal amines. The repulsive interactions hinders the formation of a single, large cluster in a localized region of the DV bilayer. Hence, the dendrons aggregate into a single cluster that decorates the surface of the DV bilayer like a mesh (as shown in Fig. 6). This organization of a single PDA cluster into a mesh is surmised to enable the redistribution of the asymmetric stresses across the DV bilayer to circumvent excessive curvature from being localized in a single region.

Since the dendron–lipid interactions decrease with increase in the size of the clusters, the terminals amines are surmised to be directed away from the DV bilayer. This configuration is observed for larger concentrations of dendrons with lower and intermediate generations for conditions where the DV remains stable.

For the PDAs with higher generations, an average cluster size of 1 is consistently observed which implies that all the dendrons are dispersed across the DV bilayer.

Impact of dendrons on the dendronized vesicle bilayer

For further insight into the stability of the DVs, the physical impact of the dendron branches on the DV bilayer is investigated. Earlier studies have developed analytical relations between the grafting density of polymers and a physical dimension of the surface[61] to determine the impact of the grafted polymer on the surface. Theoretical studies have suggested that the polymer branch imposes a lateral stress[62] on the bilayer. This stress is responsible for laterally stretching the bilayer surface, until it ruptures and disaggregates. Specifically, grafted polymers in the brush regime are reported to impose higher lateral stresses on membranes.[61,62]

To capture the lateral stretching of the surface, the volume of the outer monolayer of the DV bilayer (or, outer hydrophobic volume) is measured. The outer hydrophobic volume is the sum of the volume of all the lipid tails in the outer monolayer of the DV. The volume of the inner monolayer (or, inner hydrophobic volume) is excluded from the measurement as its expansion is not as significant as that of the outer hydrophobic volume. This is because the outer monolayer is not volumetrically constrained. A sudden increase in the hydrophobic volume is observed for DVs encompassing PDAs of intermediate generations (see Fig. 8). The significant change in the outer hydrophobic volume is observed at the critical concentration limit for this category of dendrons. The expansion of the DV outer monolayer is correlated to the physical changes observed in dendrons of intermediate generations. From the scaling measurements, dendrons of intermediate generations undergo mushroom-to-brush transitions. Hence, the conformational changes in this category of dendrons is responsible for imposing high lateral stresses on the DV bilayer. The sudden expansion of the monolayer at the critical concentration limit is potentially attributed to the mushroom-to-brush transition. This means that the grafting density at the critical concentration limit is sufficiently significant to promote the adoption of brush-like conformations by the grafted dendrons. The DV surface responds to the instantaneous effect of the lateral stresses imposed by the brush regime *via* expansion.

In the case of the stable DVs, the outer monolayer expansion due to the dendrons does not make the bilayer permeable to solvent. This is ensured by checking the packing factor of lipids in their final relaxed configurations.[63,64] All stable DVs have packing factors for the inner and outer monolayer which are within the permissible range. The packing factors for irregular-shaped DVs are observed to deviate from the permissible range. The values of the packing factor have been reported in Table S5.†

Analogous expansion effects are not observed for dendrons with lower and higher generations (see Fig. 8). This observation

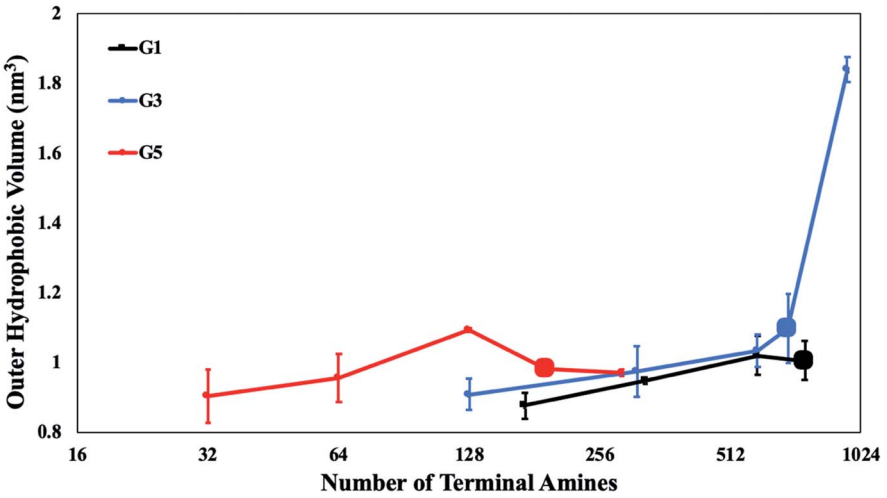

Fig. 8 The outer hydrophobic volume of the DV bilayer has been plotted against the number of terminal amines in the system. The enlarged data points represent the corresponding critical concentration limit of the dendron generation.

can be attributed to the lower tendency of the dendron conformations to transition towards the brush regime.

Fig. S1† compares the effect of long range electrostatics implemented with the PME algorithm. This experiment is performed on G3 dendrons and demonstrates that there is minimal impact of long range electrostatics. Hence, the assumption of ignoring long range electrostatics permits exploration of an extensive phase space without impacting the scientific results.

Conclusions

Disruption of quorum sensing pathways can hinder the growth of bacterial films, thereby becoming a viable mechanism for the prevention and cure of bacterial infections. Nanoparticles grafted with hyperbranched polyelectrolytes have been demonstrated to be successful in the disruption of quorum sensing pathways.[8,9] Fundamental insight into the physical mechanisms underlying the stability of these nanoparticles can yield new classes of antibacterial agents which circumvent the risk of developing resistance to antibiotics. This study provides a fundamental understanding of the physical mechanisms underlying the stability of a class of such nanoparticles, namely DVs encompassing PDAs.

The self-organization of PDAs on vesicles provides insight into the key factors which determine the stability of DVs. These factors are determined by the generation and relative concentration of the PDAs. These factors include the electrostatic interactions between dendrons; dendrons and lipids; conformational changes of the dendrons and the spontaneous curvature induced by the dendrons on the DV bilayer. An interplay of these factors dictates the stability of DVs.

DVs encompassing PDAs and DPPC molecules are generated. Variation of the relative concentration and PAMAM dendron generation yields a phase diagram for the DVs. A critical concentration limit for each dendron generation is identified. This concentration serves to differentiate between stable and unstable DVs.

Lower dendron generations (namely, G1 and G2) are observed to have large critical concentration limits. Favorable interactions between the terminally protonated amines and lipid head groups anchor the short dendron branches onto the DV surface. These interactions prevent any notable conformational change in the dendron branches, and enable the generation of stable DVs with a high concentration of PDAs with lower generations. Further, conformational restraints induce the dendritic arms to interact laterally and have their excluded volumes intrude into the corresponding excluded volumes of neighboring dendrons. This intrusion gives rise to unfavorable electrostatic repulsions between the terminally protonated amines in the branches of all the dendrons of lower generations which are distributed across the DV bilayer. This unfavorable interaction increases the spacing between the PDAs, thereby disrupting the stability of the DV bilayer. Hence, beyond a certain concentration limit, the electrostatic repulsion between the terminal amines induces the formation of transient pores in several locations in the DV bilayer, resulting in the rupture of the vesicle.

PDAs with intermediate generations (*i.e.*, G3 and G4) diffuse towards the bicelle edge during the bicelle-to-vesicle transition. Once the edges of the bicelle fuse to form a vesicle, the PDAs aggregate into a single large cluster. This cluster has the potential to induce local asymmetric stresses on the DV bilayer. In addition, this category of PDAs demonstrates mushroom-to-brush transition. The conformational change in the dendrons during the transition to the brush regime expands the DV bilayer. Hence, sufficient expansion of the bilayer due to conformational changes of the dendrons branches along with localized, highly asymmetric stresses arising due to aggregation of the dendrons ruptures the DVs.

PDAs with higher generations (*i.e.*, G5 and G6) remain dispersed in the DV bilayer. Spontaneous curvature effects associated with a single higher generation dendron causes

localized expansion of the DV bilayer. In addition, the significantly high number of dendron–lipid interactions has the potential to create pores in the DV bilayer. This observation is attributed to the high charge density of dendrons with larger generations. Since the dendrons are dispersed in the DV bilayer, the resultant asymmetric stresses in the bilayer are not minimized *via* spatial localization. Therefore, the collective impact of the spontaneous curvature induced by the PDAs along with the dendron–lipid interactions (on account of the dispersed dendrons) are surmised to rupture the DV bilayer.

These results emphasize the importance of self-organization of the PDAs in the DV bilayer. Whereas the aggregation of PDAs with lower and intermediate generations minimize asymmetric stresses in the bilayer, their localized aggregation could potentially rupture the vesicle. This situation is avoided by the electrostatic repulsion between the terminal amines, specifically for higher relative concentrations of PDAs. Hence, the dendrons self-organize into a single cluster that decorates the surface of the DV bilayer like a mesh. The mesh-like organization of the PDA cluster redistributes the asymmetric stresses across the DV bilayer, thereby circumventing its rupture.

Testing of the DV bilayer for lateral stretching provides a correlation between mushroom-to-brush transition and the expansion of the DV bilayer for PDAs with intermediate generations. These observations provide a qualitative relationship between dendron conformations and bilayer stability.

This study identifies the key factors, for each category of dendrons, which promote the rupture of DV bilayers. The critical concentration limits for each dendron generation could potentially guide the design of stable nanoparticles for anti-quorum sensing applications. An optimal choice of dendron generation could target specific quorum sensing pathways. In addition, specific conditions under which the terminal amines are exposed to the aqueous medium are noted. Nanoparticles designs adhering to these conditions could be used to electrostatically bind with charged molecules or ions in solution.[50]

Prior experimental studies have demonstrated the formation of vesicles encompassing PAMAM dendron-grafted amphiphiles.[12,13,16,17] In this study, phospholipids are mixed with similar molecules with different dendron generations. The system in this study is similar to polyethylene glycol (PEG)ylated vesicles encompassing PEG-grafted amphiphiles and phospholipids[65–67] with PEG chains substituted by the PAMAM dendrons. The presence of the dendrons endow the DVs with anti-quorum sensing functionality. Whereas, the presence of the phospholipids allow the DV to fuse with the cell membrane. Both these functionalities are non-toxic to the cell. In addition, hyperbranched polyelectrolytes have been used to deliver nucleic acids and other charged biomolecules to treat various ailments.[68–70] This demonstrates that the DVs can be used in diverse applications and therefore are highly multifunctional.

Author contributions

Akash Banerjee: formal analysis, investigation, methodology, software, supervision, validation, visualization, writing-original draft, review & editing. Acacia Tam: formal analysis, investigation, software. Meenakshi Dutt: conceptualization, funding acquisition, methodology, project administration, resources, supervision, writing-review and editing.

Conflicts of interest

There are no conflicts to declare.

Acknowledgements

M. D. would like to acknowledge NSF CAREER award DMR-1654325 and NSF REU award DMR-1659099. Portions of the research presented used computational resources supported by NSF XSEDE (allocation DMR-140125).

References

1 A. K. Bhardwaj, K. Vinothkumar and N. Rajpara, *Recent Pat. Anti-Infect. Drug Discovery*, 2013, **8**, 68–83.
2 M. Shaaban, A. Elgaml and E. S. E. Habib, *Microb. Pathog.*, 2019, **127**, 138–143.
3 Y. M. Chong, W. F. Yin, C. Y. Ho, M. R. Mustafa, A. H. A. Hadi, K. Awang, P. Narrima, C. L. Koh, D. R. Appleton and K. G. Chan, *J. Nat. Prod.*, 2011, **74**, 2261–2264.
4 M. S. A. Khan, M. Zahin, S. Hasan, F. M. Husain and I. Ahmad, *Lett. Appl. Microbiol.*, 2009, **49**, 354–360.
5 M. R. Parsek and E. P. Greenberg, *Trends Microbiol.*, 2005, **13**, 27–33.
6 F. A. Qais, M. S. Khan and I. Ahmad, in *Biotechnological Applications of Quorum Sensing Inhibitors*, 2018, pp. 227–244.
7 K. Naik and M. Kowshik, *J. Appl. Microbiol.*, 2014, **117**, 972–983.
8 R. Issa, S. T. Meikle, S. James and I. R. Cooper, *J. Mater. Sci.: Mater. Med.*, 2015, **26**, 176.
9 Y. Zhang, X. Bi, K. G. Virga, W. Chen, J. D. Gruber and B. Wang, *Mater. Sci.*, 2013, 4–9.
10 Y. Lu, D. L. Slomberg, A. Shah and M. H. Schoenfisch, *Biomacromolecules*, 2013, **14**, 3589–3598.
11 L. J. Fox, R. M. Richardson and W. H. Briscoe, *Adv. Colloid Interface Sci.*, 2018, **257**, 1–18.
12 T. Doura, M. Yamada, R. Teranishi, Y. Yamamoto, T. Sugimoto, E. Yuba, A. Harada and K. Kono, *Langmuir*, 2015, **31**, 5105–5114.
13 E. Yuba, Y. Nakajima, K. Tsukamoto, S. Iwashita, C. Kojima, A. Harada and K. Kono, *J. Controlled Release*, 2012, **160**, 552–560.
14 D. Lombardo, *Biochem. Res. Int.*, 2014, **2014**, 1–10.
15 H. Lee and R. G. Larson, *J. Phys. Chem. B*, 2008, **112**, 7778–7784.
16 T. Takahashi, C. Kojima, A. Harada and K. Kono, *Bioconjugate Chem.*, 2007, **18**, 1349–1354.
17 T. Takahashi, K. Kono, T. Itoh, N. Emi and T. Takagishi, *Bioconjugate Chem.*, 2003, **14**, 764–773.
18 M. Gosika and P. K. Maiti, *Soft Matter*, 2018, **14**, 1925–1938.
19 L. Chong, F. Aydin and M. Dutt, *J. Comput. Chem.*, 2016, **37**, 920–926.

20 Y. Kim, Y. Kwak and R. Chang, *J. Phys. Chem. B*, 2014, **118**, 6792–6802.
21 B. A. Holm, Z. Wang, E. A. Egan and R. H. Notter, *Pediatr. Res.*, 1996, **39**, 805–811.
22 A. H. de Vries, A. E. Mark and S. J. Marrink, *J. Am. Chem. Soc.*, 2004, **126**, 4488–4489.
23 W. F. D. Bennett and D. P. Tieleman, *J. Chem. Theory Comput.*, 2011, **7**, 2981–2988.
24 V. Knecht and S.-J. Marrink, *Biophys. J.*, 2007, **92**, 4254–4261.
25 H. M. K. Mohd, A. F. Ahmad, S. Radiman, F. Mohamed, N. R. A. M. Rosli, M. T. M. Ayob and I. A. Rahman, *AIP Conf. Proc.*, 2014, **1614**, 65–68.
26 S. Ohtake, C. Schebor and J. J. de Pablo, *Biochim. Biophys. Acta, Biomembr.*, 2006, **1758**, 65–73.
27 W. Chen, F. Duša, J. Witos, S.-K. Ruokonen and S. K. Wiedmer, *Sci. Rep.*, 2018, **8**, 14815.
28 M. Hossann, B. Kneidl, M. Peller, L. Lindner and G. Winter, *Int. J. Nanomed.*, 2014, 4387.
29 V. Nele, M. N. Holme, U. Kauscher, M. R. Thomas, J. J. Doutch and M. M. Stevens, *Langmuir*, 2019, **35**, 6064–6074.
30 A. Mahendra, H. P. James and S. Jadhav, *Chem. Phys. Lipids*, 2019, **218**, 47–56.
31 S. J. Marrink, H. J. Risselada, S. Yefimov, D. P. Tieleman and A. H. de Vries, *J. Phys. Chem. B*, 2007, **111**, 7812–7824.
32 W. Chen, F. Duša, J. Witos, S.-K. Ruokonen and S. K. Wiedmer, *Sci. Rep.*, 2018, **8**, 14815.
33 G. D. Bothun, *J. Nanobiotechnol.*, 2008, **6**, 13.
34 U. Essmann, L. Perera, M. L. Berkowitz, T. Darden, H. Lee and L. G. Pedersen, *J. Chem. Phys.*, 1995, **103**, 8577–8593.
35 T. Darden, D. York and L. Pedersen, *J. Chem. Phys.*, 1993, **98**, 10089–10092.
36 H. J. C. Berendsen, D. van der Spoel and R. van Drunen, *Comput. Phys. Commun.*, 1995, **91**, 43–56.
37 E. Lindahl, B. Hess and D. van der Spoel, *J. Mol. Model.*, 2001, **7**, 306–317.
38 T. A. Wassenaar, H. I. Ingólfsson, R. A. Böckmann, D. P. Tieleman and S. J. Marrink, *J. Chem. Theory Comput.*, 2015, **11**, 2144–2155.
39 H. Lee and R. G. Larson, *J. Phys. Chem. B*, 2006, **110**, 18204–18211.
40 H. Lee and R. G. Larson, *Macromolecules*, 2011, **44**, 2291–2298.
41 S. Kanchi, M. Gosika, K. G. Ayappa and P. K. Maiti, *J. Chem. Theory Comput.*, 2018, **14**, 3825–3839.
42 T. J. Prosa, B. J. Bauer, E. J. Amis, D. A. Tomalia and R. Scherrenberg, *J. Polym. Sci., Part B: Polym. Phys.*, 1997, **35**, 2913–2924.
43 K. Hong, Y. Liu, L. Porcar, D. Liu, C. Y. Gao, G. S. Smith, K. W. Herwig, S. Cai, X. Li, B. Wu, W.-R. Chen and L. Liu, *J. Phys.: Condens. Matter*, 2012, **24**, 064116.
44 G. Bussi, D. Donadio and M. Parrinello, *J. Chem. Phys.*, 2007, **126**, 014101.
45 K. Koshiyama, M. Taneo, T. Shigematsu and S. Wada, *J. Phys. Chem. B*, 2019, **123**, 3118–3123.
46 W. Shinoda, D. E. Discher, M. L. Klein and S. M. Loverde, *Soft Matter*, 2013, **9**, 11549.
47 H. E. Warriner, S. L. Keller, S. H. J. Idziak, N. L. Slack, P. Davidson, J. A. Zasadzinski and C. R. Safinya, *Biophys. J.*, 1998, **75**, 272–293.
48 S. Hong, A. U. Bielinska, A. Mecke, B. Keszler, J. L. Beals, X. Shi, L. Balogh, B. G. Orr, J. R. Baker and M. M. Banaszak Holl, *Bioconjugate Chem.*, 2004, **15**, 774–782.
49 H. Ellens, J. Bentz and F. C. Szoka, *Biochemistry*, 1986, **25**, 285–294.
50 L. Chong and M. Dutt, *Phys. Chem. Chem. Phys.*, 2015, **17**, 10615–10623.
51 H. Lee, A. H. de Vries, S.-J. Marrink and R. W. Pastor, *J. Phys. Chem. B*, 2009, **113**, 13186–13194.
52 P. G. de Gennes, in *Simple Views on Condensed Matter*, 2003, pp. 270–291.
53 O. Garbuzenko, Y. Barenholz and A. Priev, *Chem. Phys. Lipids*, 2005, **135**, 117–129.
54 R. Bartucci, M. Pantusa, D. Marsh and L. Sportelli, *Biochim. Biophys. Acta, Biomembr.*, 2002, **1564**, 237–242.
55 L. N. Gergidis, A. Kalogirou, A. Charalambopoulos and C. Vlahos, *J. Chem. Phys.*, 2013, **139**, 044913.
56 X. Yu and M. Dutt, *Mol. Syst. Des. Eng.*, 2018, **3**, 883–895.
57 B. Kollmitzer, P. Heftberger, M. Rappolt and G. Pabst, *Soft Matter*, 2013, **9**, 10877.
58 F. Aydin, G. Uppaladadium and M. Dutt, *Colloids Surf., B*, 2015, **128**, 268–275.
59 H. Lee and R. Larson, *Molecules*, 2009, **14**, 423–438.
60 S. Hong, R. Rattan, I. J. Majoros, D. G. Mullen, J. L. Peters, X. Shi, A. U. Bielinska, L. Blanco, B. G. Orr, J. R. Baker and M. M. B. Holl, *Bioconjugate Chem.*, 2009, **20**, 1503–1513.
61 D. Marsh, *Biophys. J.*, 2001, **81**, 2154–2162.
62 D. Marsh, R. Bartucci and L. Sportelli, *Biochim. Biophys. Acta, Biomembr.*, 2003, **1615**, 33–59.
63 J. N. Israelachvili, D. J. Mitchell and B. W. Ninham, *J. Chem. Soc., Faraday Trans. 2*, 1976, **72**, 1525.
64 R. Nagarajan, *Langmuir*, 2002, **18**, 31–38.
65 S. Tsuda, T. Sakakura, S. Fujii, H. Suzuki and T. Yomo, *PLoS One*, 2015, **10**, e0132963.
66 S. Khan, J. McCabe, K. Hill and P. A. Beales, *J. Colloid Interface Sci.*, 2020, **562**, 418–428.
67 M. L. Immordino, F. Dosio and L. Cattel, *Int. J. Nanomed.*, 2006, **1**, 297–315.
68 S. Chen, X.-Z. Zhang, S.-X. Cheng, R.-X. Zhuo and Z.-W. Gu, *Biomacromolecules*, 2008, **9**, 2578–2585.
69 G. Wang, H. Yin, J. C. Yin Ng, L. Cai, J. Li, B. Z. Tang and B. Liu, *Polym. Chem.*, 2013, **4**, 5297.
70 G. Feng, J. Liang and B. Liu, *Macromol. Rapid Commun.*, 2013, **34**, 705–715.